# LINEAR REFRACTION-DIFFRACTION MODEL FOR STEEP BATHYMETRY

**By Carmela N. Chandrasekera[1] and Kwok Fai Cheung[2]**

**ABSTRACT:** This paper describes the mathematical formulation, the numerical solution, and the validation of a linear refraction-diffraction model for steep bathymetry. The model involves two coupled governing equations derived from, respectively, the exact seabed boundary condition and the Laplace equation. It reduces to the extended and the original mild-slope model, when the seabed slope is small. Although the present approach is based on depth-integration of flow characteristics, it correctly accounts for the vertical component of the seabed fluid velocity. The formulation is based on the weighted-residual method, and the hybrid element solution is derived from a Galerkin approach. The capability of the present model to simulate flow velocity and wave amplitude over three-dimensional bedforms is examined in a parametric study. The computed results are compared with the original and extended mild-slope solutions and verified with those of a three-dimensional wave model. The present depth-integrated model has the same data requirements as other two-dimensional models, but provides accurate three-dimensional results with only a fraction of the CPU time that would be required by a three-dimensional model.

## INTRODUCTION

Deep ocean waves change their height and direction as they enter shoaling waters. Numerous linear and nonlinear computational models are available to predict these changes. Among the linear models, the depth-integrated refraction-diffraction equation derived by Berkhoff (1972) is one of the most commonly used. It is also known as the mild-slope equation, because its derivation is based on the assumption of gradually varying bathymetry. This elliptic partial differential equation has been solved with increasing computational efficiency and applied to model wave transformation over extensive coastal regions (e.g., Panchang et al. 1991; Oliveira and Anastasiou 1998). Numerous studies have been conducted to improve the applicability of the mild-slope equation for rapidly undulating and relatively steep bathymetry.

Kirby (1986) extended the mild-slope approximation to include rapidly varying, small amplitude deviations from a gradually varying bathymetry. Porter and Staziker (1995) proposed a matching condition to ensure the conservation of mass flow over a discontinuous seabed slope. To account for relatively steep slopes, Massel (1993) and Chamberlain and Porter (1995) used, respectively, the Galerkin eigen-function method and the variational principle to derive an extended mild-slope equation that contains additional terms proportional to the bottom curvature and the square of the slope. Chandrasekera and Cheung (1997) provided an alternative derivation of the extended equation based on Berkhoff's (1972, 1976) approach and applied their model to study wave transformation over three-dimensional bedforms and evaluate the relative significance of the curvature and slope-squared terms. Suh et al. (1997) and Lee et al. (1998) derived time-dependent and hyperbolic forms of the extended mild-slope equation.

Despite attempts to extend the mild-slope equation for steep bathymetry, the extended mild-slope equation is still based on the original assumption that the seabed slope is small. As a result, the seabed is treated as locally horizontal in the mathematical formulation, and the plane wave solution is used to describe the variation of the solution in the vertical direction. The vertical component of the fluid velocity is, therefore, always equal to zero at the seabed, regardless of its slope. For steep bathymetry, this vertical velocity is not negligible and might affect the overall water particle kinematics and wave height distribution. Furthermore, the effectiveness of these depth-integrated refraction-diffraction models has mostly been studied based on the computed wave height. Few studies have investigated the accuracy of these models in reproducing the correct water particle kinematics near the seabed, which is critical to many coastal engineering applications.

This paper presents a two-equation refraction-diffraction model that correctly accounts for the vertical component of the fluid velocity on a sloping seabed. The present model, which satisfies the exact seabed boundary condition, is more accurate in modeling wave transformation over steep bathymetry. It reduces to the one-equation mild-slope model, if the seabed slope is small. The validity of the present approach is examined through a parametric study involving three-dimensional shoals. The computed wave height and water particle velocity are compared with the results of the mild-slope model of Berkhoff (1972), the extended refraction-diffraction model of Chandrasekera and Cheung (1997), and the three-dimensional wave model of Yue et al. (1976). The applicability, computational efficiency, and accuracy of the proposed model to calculate wave transformation over steep bathymetry are evaluated and discussed.

## MATHEMATICAL FORMULATION

This section presents the derivation of two coupled governing equations for linear wave refraction-diffraction over steep bathymetry. The incident waves are assumed to be periodic and monochromatic, and the steady-state problem is formulated in the frequency domain. The three-dimensional boundary-value problem and its weighted-residual form are presented first. A new approximation procedure is introduced to allow integration of the weighted residuals in the vertical direction, while satisfying the exact seabed boundary condition. The weighted residuals defined in the two-dimensional horizontal plane provide the two governing equations and the boundary condition.

### Three-Dimensional Problem

The three-dimensional boundary-value problem is defined with a right-handed Cartesian coordinate system ($x$, $y$, $z$), in which $x$ and $y$ are measured horizontally, and $z$ is measured vertically upward from the still water level. The fluid is assumed to be incompressible and inviscid, and the flow irro-

[1]Grad. Res. Asst., Dept. of Oc. and Resour. Engrg., Univ. of Hawaii at Manoa, Honolulu, HI 96822; presently, Assoc., Philip Williams & Associates, 770 Tamalpaio Drive, Ste. 401, Corte Madera, CA 94925.

[2]Assoc. Prof., Dept. of Oc. and Resour. Engrg., Univ. of Hawaii at Manoa, Honolulu, HI (corresponding author).

Note. Discussion open until November 1, 2001. To extend the closing date one month, a written request must be filed with the ASCE Manager of Journals. The manuscript for this paper was submitted for review and possible publication on November 1, 1999; revised October 24, 2000. This paper is part of the ***Journal of Waterway, Port, Coastal, and Ocean Engineering***, Vol. 127, No. 3, May/June, 2001. ©ASCE, ISSN 0733-950X/01/0003-0161–0170/$8.00 + $.50 per page. Paper No. 22136.

tational. The fluid motion can be described by a flow potential $\Phi$

$$\Phi(x, y, z, t) = \mathrm{Re}[\phi(x, y, z)e^{-i\omega t}] \quad (1)$$

where $i = \sqrt{-1}$; $t$ = time; and $\omega$ = angular frequency. The spatially dependent potential $\phi$ satisfies the Laplace equation within the fluid domain $D$

$$\frac{\partial^2\phi}{\partial x^2} + \frac{\partial^2\phi}{\partial y^2} + \frac{\partial^2\phi}{\partial z^2} = 0 \quad (2)$$

The wave amplitude is assumed to be small, and energy dissipation is not considered. The combined free surface boundary condition can be linearized and applied at the still water level as

$$\frac{\partial\phi}{\partial z} - \frac{\omega^2}{g} = 0 \quad (3)$$

where $g$ = gravitational acceleration. The seabed is impermeable and the no-flux boundary condition can be written as

$$\frac{\partial\phi}{\partial n} = 0 \quad (4)$$

where $n$ = direction normal to a boundary surface. The scattered component of the potential satisfies the radiation condition on a vertical control surface truncating the infinite domain

$$\frac{\partial\phi^S}{\partial n} - ik\phi^S = 0 \quad (5)$$

where $\phi^S$ = scattered potential; and $k$ = wave number satisfying the linear dispersion relation.

The weighted-residual method can be applied to formulate a solution for the three-dimensional water wave problem. The method minimizes the numerical errors in the solution by equating the weighted residuals of the governing equation over the domain and the boundary conditions over the boundaries to zero. This results in

$$\iiint_D W_1\left(\frac{\partial^2\phi}{\partial x^2} + \frac{\partial^2\phi}{\partial y^2} + \frac{\partial^2\phi}{\partial z^2}\right) dV + \iint_S W_2\left(\frac{\partial\phi}{\partial z} - \frac{\omega^2}{g}\phi\right) ds$$
$$+ \iint_B W_3\frac{\partial\phi}{\partial n}\, ds + \iint_C W_4\left(\frac{\partial\phi^S}{\partial n} - ik\phi^S\right) ds = 0 \quad (6)$$

where $V$ = volume; $s$ = surface; $W_1$, $W_2$, $W_3$, and $W_4$ = weighting functions; and $S$, $B$, and $C$ indicate the still water surface, the seabed, and the control surface, respectively. The weighting functions can be arbitrary as long as the resulting integrals remain finite (e.g., Zienkiewicz and Taylor 1989).

## Two-Dimensional Approximation

The first step to eliminate the $z$ dependence in the three-dimensional boundary-value problem is to separate the flow potential $\phi$ into horizontal and vertical components. The standard approach is to represent the vertical structure of the potential by that of plane waves using the local water depth. This approximation does not entirely satisfy the seabed boundary condition and is only valid when the seabed slope is small. In the present approach, the approximation of $\phi$ contains an additional term to account more accurately for the seabed boundary condition:

$$\phi(x, y, z) \approx \varphi(x, y)Z(h(x, y), z) + \varphi_1(x, y)Z_1(h(x, y), z) \quad (7)$$

in which

$$Z(h(x, y), z) = \frac{\cosh[k(z + h)]}{\cosh(kh)} \quad (8)$$

$$Z_1(h(x, y), z) = \frac{1 - \cosh(kz)}{\cosh(kh)} \quad (9)$$

where $\varphi$ and $\varphi_1$ = flow potentials defined in the two-dimensional horizontal plane; and $h$ = water depth.

The proposed solution form, (7), satisfies the free surface boundary condition (3) and the linear dispersion relation. The first term of (7) is also known as the zeroth-order term and has been used in the derivation of the original and extended mild-slope equations. It represents the plane wave component, which has a zero vertical velocity at the seabed. The second term has a nonzero derivative with respect to $z$ at $z = -h$ and is used here to account for the vertical component of the fluid velocity on a sloping seabed. This vertical velocity is maximum at the seabed and decreases to zero at the still water level to satisfy the free surface boundary condition. The function $Z_1$ described by (9) is selected here, because it gives a linear distribution in shallow water and a more rapid decrease toward the water surface for larger values of $kh$. Other functions could be selected as long as they possess similar characteristics.

The residual of the free surface boundary condition in (6) vanishes, because of the solution form (7). With the seabed boundary condition written in terms of the water depth, the weighted-residual equation (6) becomes

$$\iint_S W_1\int_{-h}^{0} Z\left(\frac{\partial^2\phi}{\partial x^2} + \frac{\partial^2\phi}{\partial y^2} + \frac{\partial^2\phi}{\partial z^2}\right) dz\, ds$$
$$+ \iint_S W_3\left(\frac{\partial\phi}{\partial z} + \nabla\phi\cdot\nabla h\right) ds$$
$$+ \int_{\partial R} W_4\int_{-h}^{0} Z\left(\frac{\partial\phi^S}{\partial n} - ik\phi^S\right) dz\, dl = 0 \quad (10)$$

where $\nabla = (\partial/\partial x, \partial/\partial y)$; $S$ = two-dimensional domain; $\partial R$ = radiation boundary; and $l$ = distance along $\partial R$. The function $Z$ is used as the weighting function in the depth-integration to give more emphasis to the propagating mode. For arbitrary weighting functions $W_1$, $W_3$, and $W_4$, (10) is satisfied provided that

$$\int_{-h}^{0} Z\left(\frac{\partial^2\phi}{\partial x^2} + \frac{\partial^2\phi}{\partial y^2} + \frac{\partial^2\phi}{\partial z^2}\right) dz = 0 \quad (11)$$

$$\frac{\partial\phi}{\partial z} + \nabla\phi\cdot\nabla h = 0 \quad (12)$$

$$\int_{-h}^{0} Z\left(\frac{\partial\phi^S}{\partial n} - ik\phi^S\right) dz = 0 \quad (13)$$

After evaluating the depth-integration, the entire weighted-residual formulation is defined in the two-dimensional horizontal plane. Eqs. (11) and (12) give rise to the two governing equations in the horizontal plane, and (13) corresponds to the radiation condition of the two-dimensional boundary-value problem.

## Coupled Refraction-Diffraction Equations

The coupled governing equations for wave refraction-diffraction over steep bathymetry are defined in (11) and (12). We first derive the governing equation based on the seabed boundary condition, because it is already defined in the two-dimensional horizontal plane. Substitution of the solution form (7) into the seabed boundary condition (12) gives

$$Z\nabla h\cdot\nabla\varphi + (\nabla Z\cdot\nabla h)\varphi + Z_z\varphi + Z_1\nabla h\cdot\nabla\varphi_1$$
$$+ Z_{1,z}\varphi_1 + (\nabla Z_1\cdot\nabla h)\varphi_1 = 0 \quad (14)$$

where the subscript $z$ denotes partial derivative with respect to $z$. By noting that $Z_z|_{z=-h} = 0$ and substituting $z = -h$ in (14), we obtain the first governing equation:

$$b_1\nabla h\cdot\nabla\varphi - kb_2|\nabla h|^2\varphi + b_3\nabla h\cdot\nabla\varphi_1 + \frac{\omega^2}{g}[1 + b_4|\nabla h|^2]\varphi_1 = 0 \tag{15}$$

in which

$$b_1 = \frac{1}{\cosh(kh)} \tag{16}$$

$$b_2 = \frac{\sinh(kh)\sinh(2kh)}{\cosh^2(kh)[2kh + \sinh(2kh)]} \tag{17}$$

$$b_3 = \frac{1 - \cosh(kh)}{\cosh(kh)} \tag{18}$$

$$b_4 = \frac{2kh - 2\sinh(kh) + \sinh(2kh)}{2kh + \sinh(2kh)} \tag{19}$$

Fig. 1 shows the dimensionless coefficients as functions of the water depth parameter $kh$. The coefficients $b_1$ and $b_2$ are, respectively, associated with the seabed slope and the slope-squared terms of the plane wave potential $\varphi$. Both coefficients approach zero in deep water, where the seabed has negligible effects on the surface waves. The coefficients $b_3$ and $b_4$ are related to the potential $\varphi_1$ and become unity in deep water. When the water is deep or the depth is constant

$$\varphi_1 = 0 \tag{20}$$

This condition can also be applied to reflective boundaries on a locally flat bottom, over which the normal velocity is equal to zero.

The second governing equation is obtained from the depth-integration of the Laplace equation, as indicated in (11). Substituting (7), this depth-integration becomes

$$\nabla^2\varphi\int_{-h}^{0} Z^2\,dz + \nabla\varphi\cdot\int_{-h}^{0}\nabla(Z^2)\,dz + \varphi\int_{-h}^{0} Z\nabla^2 Z\,dz$$
$$+ \varphi k^2\int_{-h}^{0} Z^2\,dz + \nabla^2\varphi_1\int_{-h}^{0} ZZ_1\,dz + 2\nabla\varphi_1\cdot\int_{-h}^{0} Z\nabla Z_1\,dz$$
$$+ \varphi_1\int_{-h}^{0} Z\nabla^2 Z_1\,dz + \varphi_1\int_{-h}^{0} ZZ_{1,zz}\,dz = 0 \tag{21}$$

The second integral in (21) is difficult to evaluate in its present form and is rewritten based on Leibniz's rule of integration as

$$\nabla\varphi\cdot\int_{-h}^{0}\nabla(Z^2)\,dz = \nabla\varphi\cdot\nabla\int_{-h}^{0} Z^2\,dz - (\nabla\varphi\cdot\nabla h)Z^2|_{-h} \tag{22}$$

After evaluating the integrals, the depth-integrated Laplace equation defined in the two-dimensional horizontal plane is given by

$$\frac{CC_g}{g}\nabla^2\varphi + \left(\frac{\nabla CC_g}{g} - b_1^2\nabla h\right)\cdot\nabla\varphi + \left[\frac{k^2CC_g}{g} + f_1\nabla^2 h\right.$$
$$\left. + (f_2 + b_1b_2)|\nabla h|^2 k\right]\varphi + \frac{c_1}{k}\nabla^2\varphi_1 + 2c_2\nabla h\cdot\nabla\varphi_1$$
$$+ [c_2\nabla^2 h + kc_3|\nabla h|^2 - kc_4]\varphi_1 = 0 \tag{23}$$

where $C$ and $C_g$ are, respectively, the phase speed and group velocity; $f_1$ and $f_2$ = coefficients for the curvature and slope-squared terms as given by Chandrasekera and Cheung (1997) for the extended refraction-diffraction equation; and $c_1$, $c_2$, $c_3$, and $c_4$ are given, respectively, by

$$c_1 = \frac{\tanh(kh) - kh}{2\cosh(kh)} \tag{24}$$

$$c_2 = \{kh\cosh(kh) + kh\cosh(3kh) - 2[-(kh)^2$$
$$+ \cosh(2kh)]\sinh(kh)\}/\{[2kh + \sinh(2kh)]\cosh^2(kh)\} \tag{25}$$

$$c_3 = -\{[15 + 64(kh)^4]\cosh(kh) + 3[3 + 28(kh)^2]\cosh(3kh)$$
$$- 21\cosh(5kh) + 12(kh)^2\cosh(5kh) - 3\cosh(7kh)$$
$$+ 39kh\sinh(kh) + 160(kh)^3\sinh(kh) - 21(kh)\sinh(3kh)$$
$$+ 64(kh)^3\sinh(3kh) + 39kh\sinh(5kh) + 3kh\sinh(7kh)\}$$
$$/\{48[2kh + \sinh(2kh)]^3\cosh^2 kh\} \tag{26}$$

$$c_4 = \frac{kh + \tanh(kh)}{2\cosh(kh)} \tag{27}$$

The coefficients from (24)–(27) are plotted as functions of $kh$ in Fig. 2. Since the coefficients modify the vertical flow structure of plane waves to account for the seabed boundary conditions, their values are maximum in shallow or intermediate water and vanish in deep water. As $kh \to 0$, the solution is not senstiive to the vertical velocity on the seabed and the

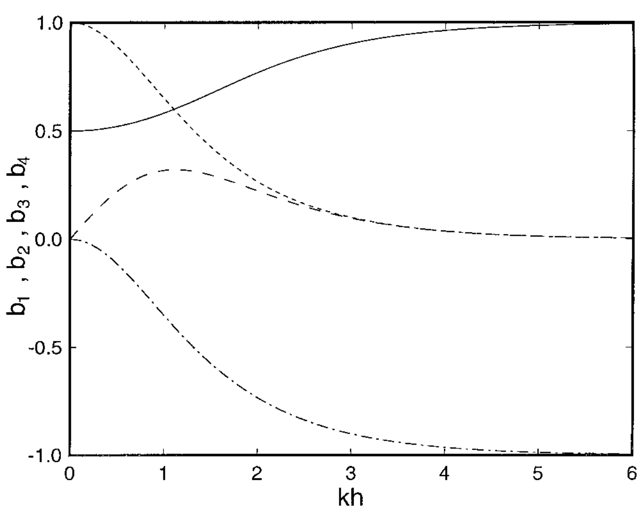


**FIG. 1.** Variation of Coefficients $b_1$, $b_2$, $b_3$, and $b_4$ with $kh$ (------, $b_1$; – – –, $b_2$; –·–, $b_3$; ——, $b_4$)

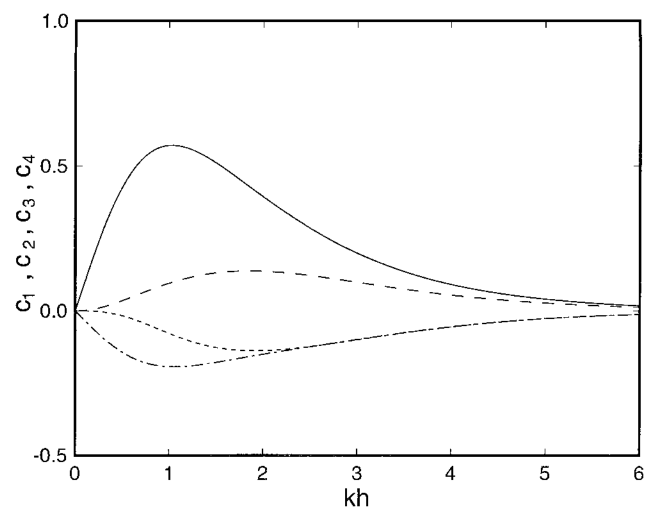


**FIG. 2.** Variation of Coefficients $c_1$, $c_2$, $c_3$, and $c_4$ with $kh$ (------, $c_1$; – – –, $c_2$; –·–, $c_3$; ——, $c_4$)

coefficients vanish. The coefficients $b_1$ and $b_2$ are present in (23), because the seabed boundary condition is not incorporated into the depth-integrated Laplace equation as in the derivations of the original and extended mild-slope equations.

The governing equations for the present refraction-diffraction model are given in (15) and (23). The two equations are coupled and must be solved simultaneously for the solution of $\varphi$ and $\varphi_1$. In addition, the solution is subjected to appropriate conditions on the lateral or open boundary, and these are treated in the numerical procedures. The two governing equations derived here are complete and can be solved using a standard numerical method. This two-equation model reduces to the one-equation extended refraction-diffraction model in the absence of the terms associated with $\varphi_1$ and becomes the mild-slope model if the terms associated with $f_1$ and $f_2$ are also omitted.

Athanassoulis and Belibassakis (1999) recently presented a linear refraction-diffraction model for steep bathymetry based on the coupled-mode approach in hydroacoustics (e.g., Fawcett 1992). The premises of their and our models are similar in that an approximation in the form of (7) is used to account for the vertical fluid velocity on a sloping seabed. However, they used a distribution equivalent to $Z_1 = (z/h)^2 + (z/h)^3$ to account for this vertical velocity and expressed the flow potential as a series of propagating and evanescent modes, which include a sloping-bottom mode. A series of coupled governing equations in the two-dimensional vertical plane are derived from the Laplace equation and the exact seabed boundary condition using the variational method. Although their governing equations can be extended to three-dimensional problems, having to solve a large number of coupled equations simultaneously may limit the practical application of their approach due to high computational and memory requirements. The present method, on the other hand, follows the weighted-residual approach and derives two governing equations from the Laplace equation and the exact seabed boundary condition, and it provides a more efficient approach to simulate wave transformation over arbitrary bathymetry in three dimensions.

## NUMERICAL FORMULATION

The numerical formulation is summarized in the weighted-residual equation, (10), which includes integration of the two governing equations in the two-dimensional horizontal plane and the radiation condition along the open boundary. A finite-element equation can be derived directly from the seabed boundary residual. The domain and open boundary residuals are treated together using the hybrid element method of Chen and Mei (1974) and provide a second finite-element equation for the two unknown potentials.

### Hybrid-Element Method

The hybrid-element method divides the domain $S$ into an inner region $A$ and an outer region $R$, as shown in Fig. 3. In the inner region, the variation of the bathymetry is significant and the solution to the governing equations is approximated by finite elements. The water depth in the outer region is either constant or too large to affect wave propagation. As a result, the potential $\varphi_1$ vanishes and the potential $\varphi$ can be represented by an analytical function. Continuity of the pressure and normal velocity along the boundary $\partial A$ separating the regions $A$ and $R$ requires that

$$\left(\frac{CC_g}{g}\,\varphi\right)_R - \left(\frac{CC_g}{g}\,\varphi\right)_A = 0 \tag{28}$$

and

$$\left(\frac{CC_g}{g}\,\frac{\partial\varphi}{\partial n_A}\right)_A - \left(\frac{CC_g}{g}\,\frac{\partial\varphi}{\partial n_A}\right)_R = 0 \tag{29}$$

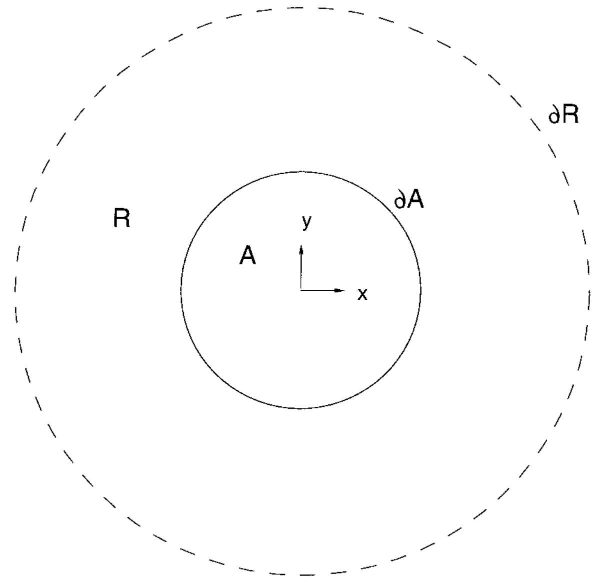


**FIG. 3.** Definition Sketch of Two-Dimensional Problem

where $n_A$ is directed outward from $A$. The flow potential $\varphi$ in the outer region can be separated into the incident and scattered components. The incident potential $\varphi^I$ is known, and the scattered potential $\varphi^S$ must satisfy the Laplace equation and the radiation condition.

The depth-integration of the Laplace equation, (11), in the outer domain $R$ gives rise to the Helmholtz equation for the scattered potential

$$\frac{CC_g}{g}\,\nabla^2\varphi^S + \frac{\nabla CC_g}{g}\cdot\nabla\varphi^S + \frac{k^2CC_g}{g}\,\varphi^S = 0 \tag{30}$$

The depth-integration of the radiation condition, (13), on the boundary $\partial R$ becomes

$$-\frac{CC_g}{g}\,\frac{\partial\varphi^S}{\partial n_R} + \frac{CC_g}{g}\,ik\varphi^S = 0 \tag{31}$$

where $n_R$ is directed outward from $R$. If the matching boundary $\partial A$ is a circular arc, the scattered potential satisfying the Helmholtz equation and the radiation condition can be expressed as

$$\varphi^S = \sum_{n=0}^{\infty} H_n(kr)(\alpha_n \cos n\theta + \beta_n \sin n\theta) \tag{32}$$

where $\alpha_n$ and $\beta_n$ = unknown coefficients; and $H_n$ = Hankel function.

### Seabed Boundary Residual

The finite-element formulation of the seabed boundary residual is straightforward and is given directly by the second term of (10). With the seabed boundary condition represented by (15), the residual becomes

$$\iint_A [b_1\nabla h\cdot\nabla\varphi - kb_2|\nabla h|^2\varphi + b_3\nabla h\cdot\nabla\varphi_1 + \frac{\omega^2}{g}(1 + b_4|\nabla h|^2)\varphi_1]W_3\,dA = 0 \tag{33}$$

There is no need to extend this integration into the outer region $R$, because the analytical solution of $\varphi$ satisfies the seabed boundary condition and the potential $\varphi_1 = 0$. The condition (20) is automatically satisifed on the boundary $\partial A$, which has a constant depth.

In this study, the inner region $A$ is composed of six-node triangular elements based on the isoparametric formulation. In each element, the potentials $\varphi$ and $\varphi_1$ and their derivatives are respectively approximated by

$$\varphi = \sum_{j=1}^{6} N_j\varphi_j, \quad \nabla\varphi = \sum_{j=1}^{6} \nabla N_j\varphi_j \tag{34a,b}$$

$$\varphi_1 = \sum_{j=1}^{6} N_j\varphi_{1j}, \quad \nabla\varphi_1 = \sum_{j=1}^{6} \nabla N_j\varphi_{1j} \tag{35a,b}$$

where $N_j$ = quadratic shape functions; and $\varphi_j$ and $\varphi_{1j}$ = values of the potentials at the nodes. The water depth and its gradient and curvature at any point within an element can be calculated from the known water depths defined at the nodes through the use of the same shape functions. Since quadratic isoparametric elements are used, the sides of the triangles are not necessarily straight lines; therefore, curved boundaries can be represented more accurately.

In the Galerkin finite-element formulation, the shape function $N_i$ is used as the weighting functions. With the values of $\varphi$ and $\varphi_1$ and their derivatives expressed by (34) and (35), the Galerkin approximation of the residual (33) can be written as a system of linear equations:

$$[X_1]\{\varphi_1\} + [Y_1]\{\varphi\} = \{0\} \tag{36}$$

where $[X_1]$ and $[Y_1]$ = square coefficient matrices, which are sparse and banded. Eq. (36) provides a relation between the potentials $\varphi$ and $\varphi_1$ based on the exact seabed boundary condition, which is not considered in the extended and original mild-slope models.

## Domain and Open Boundary Residuals

The depth-integrated Laplace equation, (23), is not self-adjoint. The variational approach that was used in the original hybrid-element method to derive the functional is not directly applicable here. The Galerkin approach is therefore used to derive the finite-element equations. Based on the governing equation (23) in $A$ and the matching conditions (28) and (29) on $\partial A$, the first and last integrals in (10) become

$$\begin{aligned}
&-\iint_A N_i \left\{\frac{CC_g}{g}\nabla^2\varphi + \left(\frac{\nabla CC_g}{g} - b_1^2\nabla h\right)\cdot\nabla\varphi \right.\\
&+ \left[\frac{k^2CC_g}{g} + f_1\nabla^2 h + (f_2 + b_1b_2)|\nabla h|^2 k\right]\varphi + \frac{c_1}{k}\nabla^2\varphi_1\\
&\left. + 2c_2\nabla h\cdot\nabla\varphi_1 + [c_2\nabla^2 h + kc_3|\nabla h|^2 - kc_4]\varphi_1\right\} dA\\
&+ \int_{\partial A} M_i\left[\left(\frac{CC_g}{g}\varphi\right)_R - \left(\frac{CC_g}{g}\varphi\right)_A\right] dl\\
&+ \int_{\partial A} N_i\left[\left(\frac{CC_g}{g}\frac{\partial\varphi}{\partial n_A}\right)_A - \left(\frac{CC_g}{g}\frac{\partial\varphi}{\partial n_A}\right)_R\right] dl = 0
\end{aligned} \tag{37}$$

where $M_i$ is a weighting function. Since an analytical solution for $\varphi$ is used in $R$, the Helmholtz equation (30) over $R$ and the radiation condition (31) over $\partial R$ are satisfied automatically. The two matching conditions connect the numerical solution in the inner region $A$ with the analytical solution in the outer region $R$.

As part of the weighted-residual method, the higher order derivatives of the unknown variables are expanded into lower order terms. Using Green's first identity, the integral involving the second-order derivative of the potential $\varphi$ in (37) can be reduced to

$$\begin{aligned}
&-\iint_A N_i\frac{CC_g}{g}\nabla^2\varphi\, dA = \iint_A \frac{CC_g}{g}\nabla N_i\cdot\nabla\varphi\, dA\\
&+ \iint_A N_i\frac{\nabla CC_g}{g}\cdot\nabla\varphi\, dA - \int_{\partial A} N_i\frac{CC_g}{g}\frac{\partial\varphi}{\partial n_A}\, dl
\end{aligned} \tag{38}$$

The boundary term represents the matching normal velocity on $\partial A$ and is a natural boundary condition in the weighted-residual formulation. It is also part of the continuation of mass flux at the boundary and can account for fully reflective boundaries on a locally flat seabed. Similarly, the second-order derivative term of $\varphi_1$ in (37) can be expressed as

$$\begin{aligned}
&-\iint_A N_i\frac{c_1}{k}\nabla^2\varphi_1\, dA = \iint_A \frac{c_1}{k}\nabla N_i\cdot\nabla\varphi_1\, dA\\
&+ \iint_A N_i\nabla\left(\frac{c_1}{k}\right)\cdot\nabla\varphi_1\, dA - \int_{\partial A} N_i\frac{c_1}{k}\frac{\partial\varphi_1}{\partial n_A}\, dl
\end{aligned} \tag{39}$$

Along the boundary $\partial A$, the water depth is constant and the potential $\varphi_1 = 0$; therefore, the boundary integral in (39) vanishes.

The residuals of the continuity equations of mass flux and pressure over $\partial A$ in (37) can be expressed in terms of the incident and scattered potentials as

$$\begin{aligned}
&\int_{\partial A} M_i\left[\left(\frac{CC_g}{g}\varphi\right)_R - \left(\frac{CC_g}{g}\varphi\right)_A\right] dl = \int_{\partial A} M_i\frac{CC_g}{g}\varphi^S\, dl\\
&+ \int_{\partial A} M_i\frac{CC_g}{g}\varphi^I\, dl - \int_{\partial A} M_i\frac{CC_g}{g}\bar\varphi\, dl
\end{aligned} \tag{40}$$

$$\begin{aligned}
&\int_{\partial A} N_i\left[\left(\frac{CC_g}{g}\frac{\partial\varphi}{\partial n_A}\right)_A - \left(\frac{CC_g}{g}\frac{\partial\varphi}{\partial n}\right)_R\right] dl = \int_{\partial A} N_i\frac{CC_g}{g}\frac{\partial\bar\varphi}{\partial n_A}\, dl\\
&- \int_{\partial A} N_i\frac{CC_g}{g}\frac{\partial\varphi^S}{\partial n_A}\, dl - \int_{\partial A} N_i\frac{CC_g}{g}\frac{\partial\varphi^I}{\partial n_A}\, dl
\end{aligned} \tag{41}$$

where $\bar\varphi$ = unknown potential on the boundary $\partial A$.

Substituting (38)–(41) into the weighted-residual equation, (37), we obtain

$$\begin{aligned}
&\iint_A \frac{CC_g}{g}\nabla N_i\cdot\nabla\varphi\, dA + \iint_A N_i b_1^2\nabla h\cdot\nabla\varphi\, dA\\
&- \iint_A N_i\left[\frac{k^2CC_g}{g} + f_1\nabla^2 h + (f_2 + b_1b_2)|\nabla h|^2 k\right]\varphi\, dA\\
&+ \iint_A \frac{c_1}{k}\nabla N_i\cdot\nabla\varphi_1\, dA + \iint_A N_i\nabla\frac{c_1}{k}\cdot\nabla\varphi_1\, dA\\
&- \iint_A 2c_2N_i\nabla h\cdot\nabla\varphi_1\, dA - \iint_A N_i(c_2\nabla^2 h + kc_3|\nabla h|^2 - kc_4)\varphi_1\, dA\\
&+ \int_{\partial A} M_i\frac{CC_g}{g}\varphi^S\, dl - \int_{\partial A} M_i\frac{CC_g}{g}\bar\varphi\, dl - \int_{\partial A} N_i\frac{CC_g}{g}\frac{\partial\varphi^S}{\partial n_A}\, dl\\
&- \int_{\partial A} N_i\frac{CC_g}{g}\frac{\partial\varphi^I}{\partial n_A}\, dl + \int_{\partial A} M_i\frac{CC_g}{g}\varphi^I\, dl = 0
\end{aligned} \tag{42}$$

Although the five boundary integrals in (42) are derived from the Galerkin method, they can be shown to be equivalent to those derived by Tsay and Liu (1983) using the variational approach. In the numerical solution, the weighting functions $M_i$ on the matching boundary are taken as the coefficients of $\alpha_i$ and $\beta_i$ from the derivative of (32) with respect to $n$.

Using the finite-element approximations (34) and (35), the weighted-residual equation (42) is reduced to a system of linear equations in terms of the unknown values of $\varphi$ and $\varphi_1$ at the nodes as well as the unknown coefficients $\alpha_i$ and $\beta_i$ associated with the scattered potential. The system of equations can be expressed in matrix form as

$$[Y_2]\{\varphi\} + [X_2]\{\varphi_1\} + [K_2]\{\mu\} + [K_1]\{\mu\} + [K_1]^T\{\bar{\varphi}\}$$

$$= \{\{Q_1\}, \{Q_2\}\} \tag{43}$$

where $\{\mu\} = \{\alpha_i, \beta_i\}$; $[Y_2]$ and $[X_2]$ = sparse square matrices; $[K_1]$ is only associated with the boundary terms; $[K_2]$ is a diagonal matrix; and $\{\{Q_1\}, \{Q_2\}\}$ = forcing vector derived from the last two integrals of (42), which contains the incident wave conditions on the boundary $\partial A$. Following the method of Chen and Mei (1974), the unknown coefficients of the analytical solution $\{\mu\}$ can be eliminated from the matrix equation, (43), giving rise to

$$[X_2]\{\varphi_1\} + [K]\{\varphi\} = \{Q\} \tag{44}$$

in which $[K]$ is a square matrix; and $\{Q\}$ is the known input vector, given, respectively, as

$$[K] = [Y_2] - [K_1][K_2]^{-1}[K_1]^T \tag{45}$$

$$\{Q\} = \{Q_1\} - [K_1][K_2]^{-1}\{Q_2\} \tag{46}$$

The unknown vector $\{\bar{\varphi}\}$ on $\partial A$ is now considered as a subset of $\{\varphi\}$. The boundary nodes are arranged at the end of the vector $\{\varphi\}$ to improve the computational efficiency.

The two finite-element equations (36) and (44) are coupled and combined to give a system of simultaneous equations in terms of $\varphi$ and $\varphi_1$ as

$$\begin{bmatrix} X_1 & Y_1 \\ X_2 & K \end{bmatrix} \begin{Bmatrix} \varphi_1 \\ \varphi \end{Bmatrix} = \begin{Bmatrix} 0 \\ Q \end{Bmatrix} \tag{47}$$

where the right-hand-side input vector is determined from the incident wave conditions. The rank of the final matrix equation (47) is twice that of the original or extended mild-slope equation model with the same number of nodes. However, the left-hand-side matrix is sparse and can efficiently be solved using an iterative method. Once the solution of the potential $\varphi$ and $\varphi_1$ are obtained from (47), the vertical velocity distribution can be evaluated from (7).

## RESULTS AND DISCUSSION

The validity of the present approach and its application to steep three-dimensional bathymetry are examined through a parametric study. The wave height and flow velocity over a circular shoal are calculated from the present coupled model and compared with those obtained from the original and extended mild-slope models as well as the three-dimensional wave model of Yue et al. (1976). The origin of the coordinate system $(x, y)$ is placed at the center of the circular shoal and the incident waves propagate in the positive $x$ direction. The water depth on the shoal at a distance $r$ from the center is given by

$$h = h_0 - \frac{b}{2}\left[\cos\left(\frac{\pi r}{R}\right) + 1\right] \text{ for } r \le R \tag{48}$$

where $h_0$ = constant water depth outside the shoal; and $R$ and $b$ = respectively, the radius and height of the shoal. The shoal has a slope ranging from zero at $r = 0$ and $R$ to the maximum $\pi b/2R$ at $r = R/2$. Two configurations are considered: $b/R$ = 0.2 and $b/h_0$ =0.4; and $b/R$ = 0.4 and $b/h_0$ = 0.8. It should be noted that the slope of this shoal is continuous. Although the method of Porter and Staziker (1995) can be applied to treat discontinuous bathymetry, we select this shoal so that we can focus our attention on the performance of the model with steep bathymetry.

### Computational Considerations

The computational domain is circular, with the shoal located at the center and the matching boundary at a distance of 1.5$R$ from the center. The 20-node hexahedral element of the ''serendipity'' family is used in the three-dimensional model. Both the two- and three-dimensional models have been tested for their sensitivity with respective to the grid and domain sizes (Chandrasekera 2000). For the results presented in this paper, at least 20 nodes are used to model a wavelength in the two-dimensional models and 10 nodes for the three-dimensional model. Five hexahedral elements are used to resolve the vertical variation of the solution in the three-dimensional model. These resolutions are higher than those required for practical applications, but are used here to produce highly accurate numerical results for this comparative study.

The computation was performed on a Pentium III 500 MHz PC with 256 MB of memory. Table 1 shows the CPU times required for solving the mild-slope, the extended refraction-diffraction, and the present models. All three models are

**TABLE 1.** Comparison of CPU Times for Two-Dimensional Models

| Number of nodes | CPU Time (min) Mild-slope | Extended | Present |
|---|---|---|---|
| 2,000 | 0.2 | 0.2 | 0.7 |
| 4,000 | 0.7 | 0.7 | 3.4 |
| 6,000 | 1.3 | 1.4 | 5.8 |
| 8,000 | 2.4 | 2.7 | 8.8 |
| 10,000 | 4.0 | 4.5 | 12.6 |

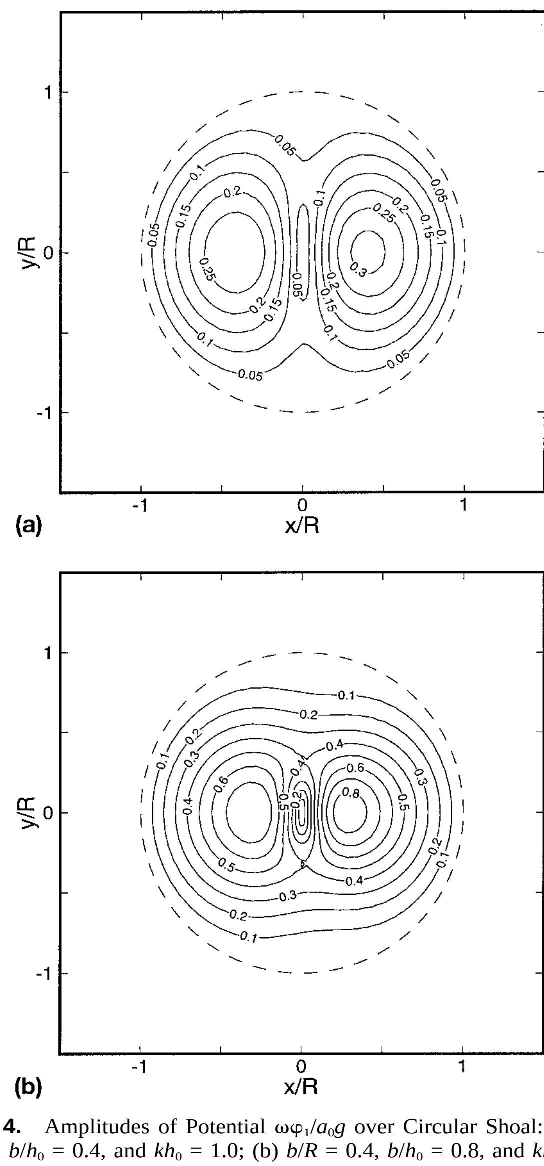


**FIG. 4.** Amplitudes of Potential $\omega\varphi_1/a_0 g$ over Circular Shoal: (a) $b/R$ = 0.2, $b/h_0$ = 0.4, and $kh_0$ = 1.0; (b) $b/R$ = 0.4, $b/h_0$ = 0.8, and $kh_0$ = 1.0

solved using a conjugate gradient solver specially adapted for complex sparse matrices. The physical problem corresponds to the configuration $b/R$ = 0.4 and $b/h_0$ = 0.8 and the wave conditions $kh_0$ = 1. The computations were performed for the same domain but with increasing resolution to yield different numbers of nodes. The results show that all three models are highly efficient and can easily be solved on a PC even for a problem with 10,000 nodes. The extended mild-slope model has slightly higher computational requirements compared with the original mild-slope model, as already discussed in Chandrasekera and Cheung (1997). The present model requires more CPU time, because twice as many unknowns are involved, but the increase is reasonable.

The present model can be viewed as a three-dimensional model with two layers of nodes: one at the water surface and the other at the seabed. The variation of the solution in the vertical direction follows the analytical functions $Z$ and $Z_1$ in (7). For the model of Yue et al. (1976), the use of 1,905 nodes at the water surface and five elements in the vertical direction results in a total of 14,635 nodes and a CPU time of 15.5 min using a banded matrix solver. The present model with 2,000 nodes on the water surface requires 0.7 min of CPU time on the same machine. The increase in CPU time and storage requirements of the three-dimensional model is much more dramatic for a higher number of nodes. Furthermore, the generation of a three-dimensional finite-element grid involving realistic bathymetry and coastlines over an extensive region is not a trivial task. The input data preparation time, which is crucial to engineering applications, is much shorter for a two-dimensional model. The present two-dimensional model, which can produce three-dimensional results with comparable data preparation time to the mild-slope model, has many engineering applications.

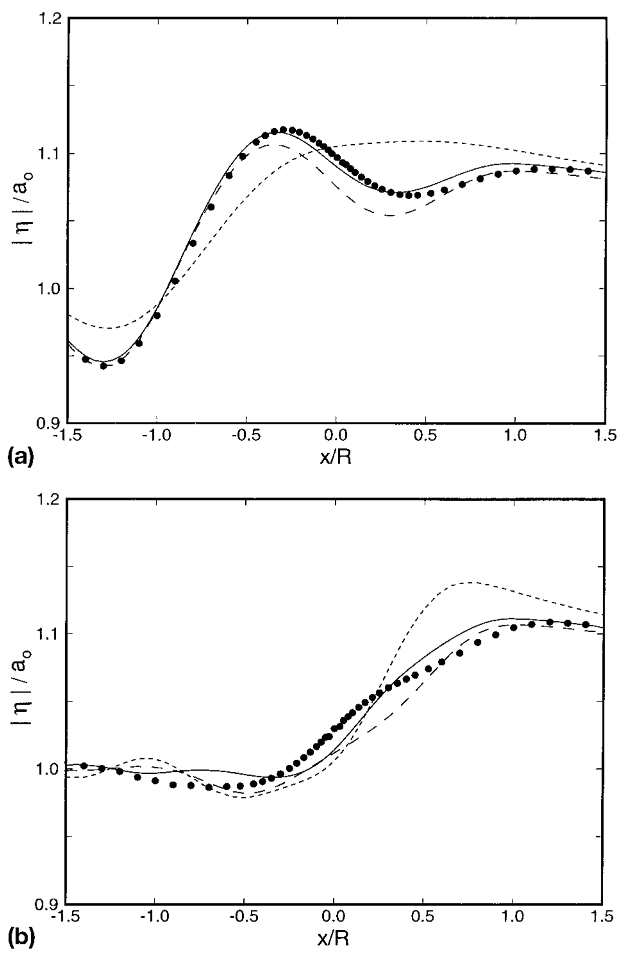


**FIG. 5.** Wave Amplitudes over Circular Shoal for $b/R$ = 0.2 and $b/h_0$ = 0.4: (a) $kh_0$ = 1.0; (b) $kh_0$ = 2.0 (------, Mild-Slope Equation; – – – –, Extended Mild-Slope Equation; ——, Present Model; ●, Three-Dimensional Model)

## Seabed Boundary Correction

The present approach uses the potential $\varphi_1$ to satisfy the seabed boundary condition and subsequently to calculate the vertical component of the fluid velocity on the seabed. The role of this potential in the solution of the present model is examined in this section. Fig. 4(a) shows the amplitude plot of the potential $\omega\varphi_1/a_0 g$ for $b/R$ = 0.2, $b/h_0$ = 0.4, and $kh_0$ = 1, where $a_0$ denotes incident wave amplitude. The amplitude of the potential is highest along the $x$ axis, because the flow is in the direction of the maximum slope and the vertical component of the seabed fluid velocity is significant. The amplitude decreases rapidly in the circumferential direction of the shoal and becomes minimum along the $y$ axis, where the local wave propagation direction is almost tangent to the shoal contours and, therefore, the correction to the seabed vertical fluid velocity is small.

The results for $b/R$ = 0.4, $b/h_0$ = 0.8, and $kh_0$ = 1 are presented in Fig. 4(b). Because this shoal has a larger average slope, the vertical fluid velocity on the shoal and subsequently the amplitude of the potential $\varphi_1$ are higher in comparison with the results in Fig. 4(a). The waves are also refracted to a greater extent due to the larger slope. Along the $y$ axis, the waves cross the contours of the shoal at greater angles, resulting in greater vertical fluid velocity on the shoal and relatively higher amplitude of the potential $\varphi_1$. In Figs. 4(a and b), the amplitude of the potential $\varphi_1$ is zero at the top of the

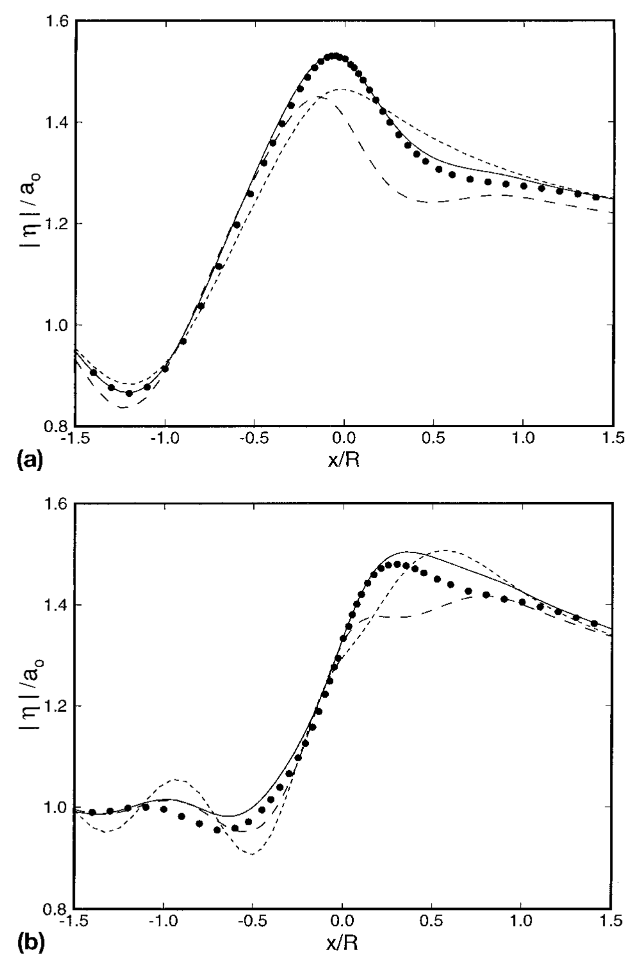


**FIG. 6.** Wave Amplitudes over Circular Shoal for $b/R$ = 0.4 and $b/h_0$ = 0.8: (a) $kh_0$ = 1.0; (b) $kh_0$ = 2.0 (See Fig. 5 Caption for Legend)

shoal and on the flat seabed immediately outside the shoal in accordance with the formulation. The potential, however, does not necessarily become maximum at $r/R = \pm 0.5$, where the slope is maximum. This is because the distribution of the potential $\varphi_1$ also depends on the local water depth as well as the refracted wave amplitude and direction.

## Wave Amplitude Distribution

The wave amplitude computed by the present model is compared with those obtained from the original and extended mild-slope models as well as the three-dimensional wave model. Although the potential $\varphi_1$ vanishes at the still water level, it affects the wave amplitude distribution over the entire computational domain through its coupling with $\varphi$ in the two governing equations. The wave amplitudes along the $x$ axis, normalized by the incident wave amplitude, are shown in Fig. 5 for the shoal configuration $b/R = 0.2$ and $b/h_0 = 0.4$ and in Fig. 6 for $b/R = 0.4$ and $b/h_0 = 0.8$. Two incident wave conditions corresponding to $kh_0 = 1$ and 2 are considered. The three-dimensional model results, which do not involve any assumption on the distribution of the solution in the vertical direction, are used here as a reference to assess the validity of the three depth-integrated models.

The wave amplitudes computed by the present model are noticeably different from those of the other two depth-integrated models. In comparison with the results of the mild-slope model, the present and the extended models consistently give lower predictions of the wave height behind the top of the shoal. This can be explained by the modification of the local wave number and the refractive focusing of the waves by the curvature term in the governing equations (Lee 1999). In comparison with the three-dimensional model results, the extended mild-slope model appears to overcorrect this effect. When $kh_0 = 1$, the present model gives very good agreement with the three-dimensional model for both shoal configurations. Although the present model slightly overestimates the wave height behind the top of the shoal for $kh_0 = 2$, its results are still better than those of the original and extended mild-slope models.

## Velocity Profile

The most important characteristic of the present model is that is satisfies the exact seabed boundary condition. This gives better predictions of the overall flow kinematics through coupling with the Laplace equation. This section examines the capability of the present model to correctly reproduce the fluid velocity above a sloping seabed. Fig. 7 shows profiles of the horizontal and vertical velocities, denoted by $u$ and $w$, respectively, at $x/R = -1.0$, $-0.5$, 0.0, and 0.5, in the $x$-$z$ plane. The results are presented for the shoal with $b/R = 0.4$ and $b/h_0 = 0.8$ and for the wave condition $kh_0 = 1.0$.

The improvement on the prediction of both the horizontal and vertical fluid velocities by the present approach is evident. Both the original and extended mild-slope models fail to reproduce the correct velocities over a significant portion of the water columns at $x/R = -0.5$ and 0.5, where the shoal has a maximum slope of 0.63. Despite the use of a simple vertical distribution for the potential $\varphi_1$, the results obtained from the

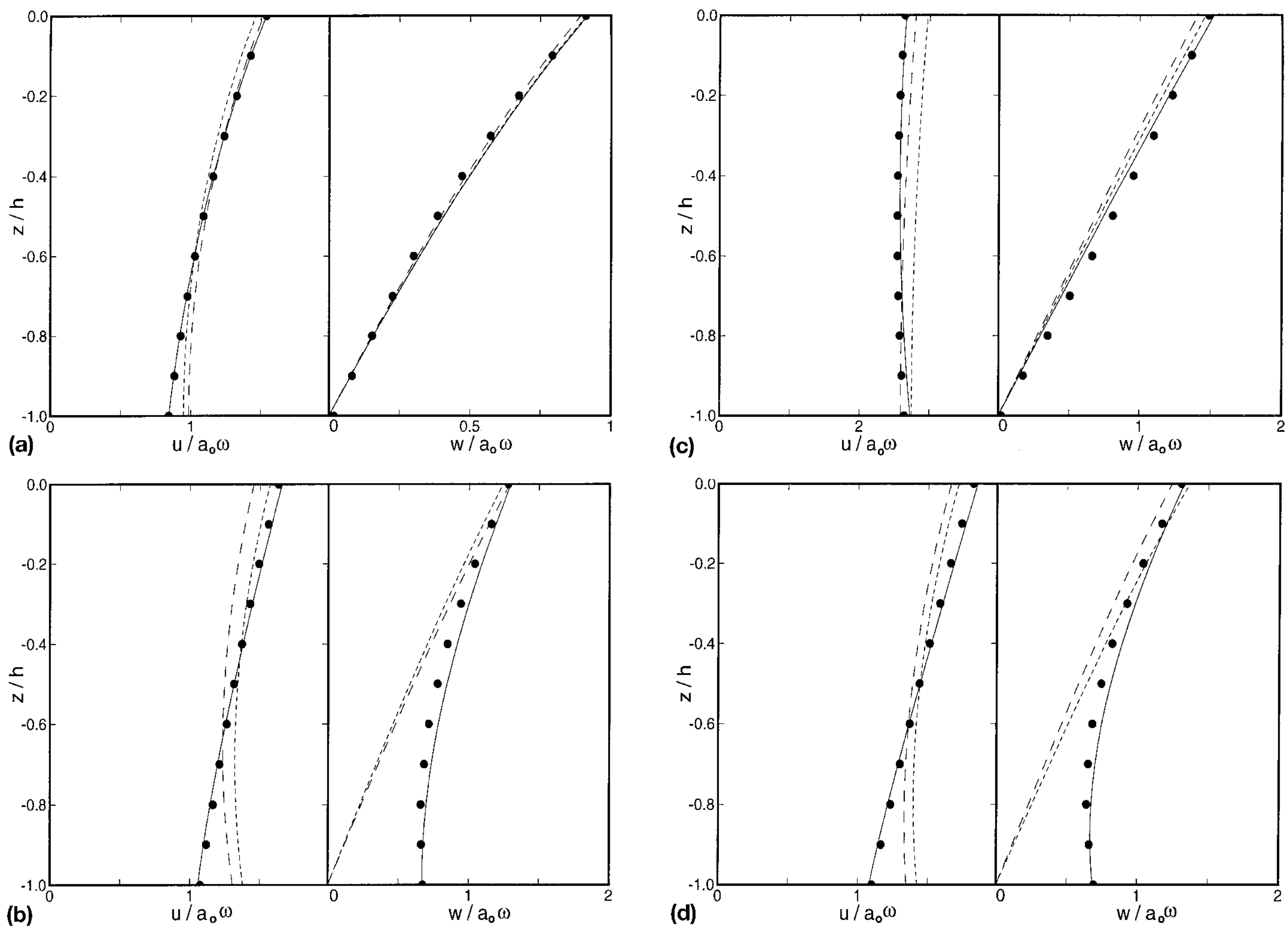


**FIG. 7.** Amplitudes of Horizontal and Vertical Velocity as Functions of $z/h$ for $b/R = 0.4$, $b/h_0 = 0.8$ and $kh_0 = 1.0$: (a) $x/R = -1.0$; (b) $x/R = -0.5$; (c) $x/R = 0.0$; (d) $x/R = 0.5$ (See Fig. 5 Caption for Legend)

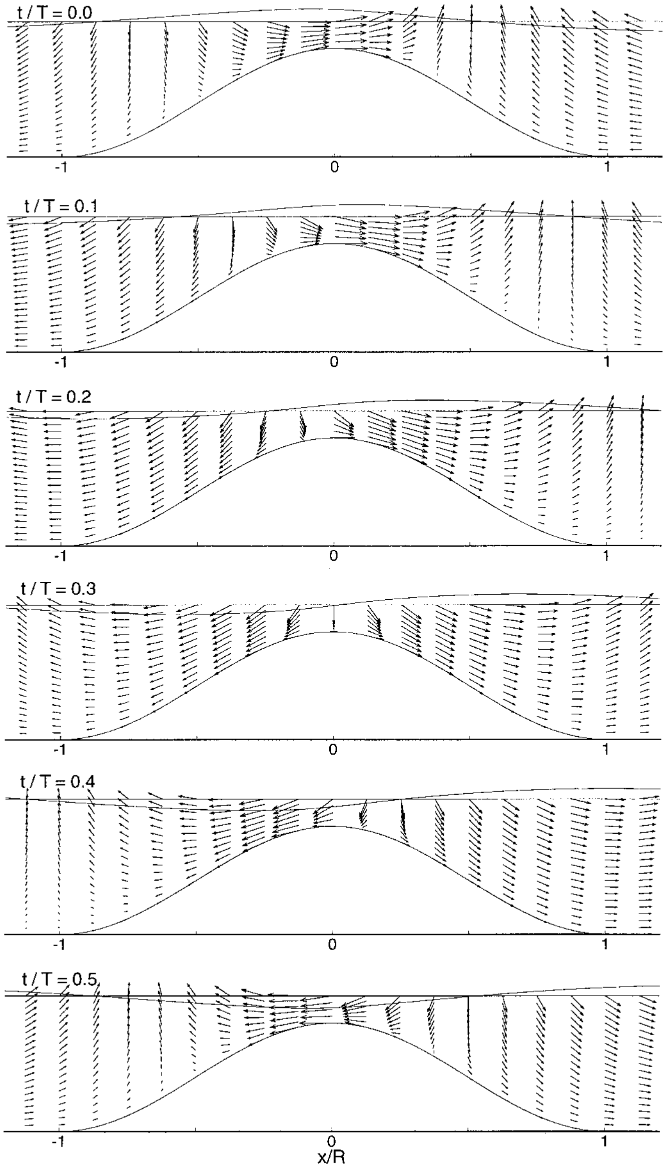


**FIG. 8.** Velocity Field in *x-z* Plane for $b/R = 0.4$, $b/h_0 = 0.8$, and $kh_0 = 1.0$

present model give good agreement with the three-dimensional model results over the entire water column. Although the primary purpose of the present model is to correctly account for the vertical velocity above a sloping seabed, it improves the horizontal velocity as well. In fact, the horizontal velocity obtained by the present model is almost identical to the three-dimensional result. All four models produce similar distributions of the velocity at the edge and the top of the shoal ($x/R = -1.0$ and 0), where the slope is zero. This indicates that the present model can be applied to a wide range of conditions and produces results that are consistent with the mild-slope model, when the seabed slope is small or negligible.

For the same shoal configuration and wave conditions, Fig. 8 shows the velocity fields in the *x-z* plane predicted by the present model over one half of a wave period (denoted by $T$). The surface wave profiles are also presented in the figure for reference. The shoal and the flow fields are shown in proportional scale and the length and direction of each arrow indicate, respectively, the magnitude and direction of the fluid velocity. The velocity vectors closely follow the shoal profile, indicating that the solution satisfies the seabed boundary condition. The effect of the sloping seabed on the flow velocity decreases toward the water surface due to the hyperbolic distribution in the second term of (7). Unlike a plane wave solution, the phase angle of the water particle velocity over the shoal varies in the vertical direction and the horizontal flow direction over some of the water columns reverses toward the seabed. Comparison of the flow velocities in Fig. 7 and the illustration of the flow fields in Fig. 8 shows that the present approach is capable of predicting realistic and accurate flow kinematics above a sloping seabed.

## CONCLUSIONS

Two linear governing equations for wave refraction-diffraction over steep bathymetry have been derived from the Laplace equation and the exact seabed boundary condition. The two equations are coupled and involve two flow potentials corresponding, respectively, to the plane-wave component with a zero vertical velocity at the seabed and a correction term accounting for the vertical fluid velocity on a sloping seabed. When the seabed slope is small, the latter component vanishes and the two equations reduce to the extended or the original mild-slope equation. The governing equations can be readily applied to steep bathymetry and solved by a standard numerical method.

The two governing equations along with the radiation condition constitute the weighted-residual formulation of the boundary-value problem in the horizontal plane. Because the mathematical problem is not self-adjoint, two systems of finite-element equations are derived by a Galerkin formulation of the hybrid-element method. The present coupled model is analogous to a linear three-dimensional model with two layers of nodes and an analytical solution in between. Its computational requirements are higher than those of the original and extended mild-slope equations, but are much less compared with a three-dimensional model with the same horizontal resolution. Most importantly, the data preparation time required by the present model is much less compared with that of a three-dimensional model, thereby enhancing its practical usefulness.

The capability of the present model to simulate wave transformation over three-dimensional bedforms is examined in a parametric study. The computed results are compared with those of a three-dimensional wave model as well as the extended and original mild-slope models. Both the extended and original mild-slope models fail to correctly evaluate the vertical fluid velocity over a significant portion of the water column above a steep shoal. The present model provides consistently better predictions of the wave amplitude and water particle kinematics as compared with the mild-slope models. The present depth-integrated model provides results that are comparable to those of a three-dimensional model, but without the need to solve the actual three-dimensional boundary-value problem.

## ACKNOWLEDGMENTS

This publication is funded in part by a grant/cooperative agreement from the National Oceanic and Atmospheric Administration (NOAA), Project No. R/EP-2, which is sponsored by the University of Hawaii Sea Grant College Program, School of Ocean and Earth Science and Technology, under Institutional Grant No. NA36RG0507 from the NOAA Office of Sea Grant, Department of Commerce. Additional financial support for this project is provided by the State of Hawaii, Department of Defense, and the National Aeronautics and Space Administration (NASA), Office of Earth Science, Grant No. NAG5-8748. The writers are thankful to these agencies for their support and, also, to Prof. Philip L.-F. Liu and Dr. Nicholas Dodd for their comments and suggestions on the manuscript. The views expressed herein are those of the writers and do not necessarily reflect the views of NOAA, NASA, or any of their subagencies. UNIHI-SEAGRANT-JC-00-02. SOEST Contribution No. 5257.

## REFERENCES


Athanassoulis, G. A., and Belibassakis, K. A. (1999). ''A consistent coupled-mode theory for the propagation of small-amplitude water waves over variable bathymetry regions.'' *J. Fluid Mech.*, 389, 275–301.

Berkhoff, J. C. W. (1972). ''Computation of combined refraction-diffraction.'' *Proc., 13th Int. Conf. on Coast. Engrg.*, ASCE, Vancouver, Canada, 1, 471–490.

Berkhoff, J. C. W. (1976). *Mathematical models for simple harmonic linear water waves: wave diffraction and refraction*, Delft Hydraulic Laboratory, Delft, The Netherlands.

Chamberlain, P. G., and Porter, D. (1995). ''The modified mild-slope equation.'' *J. Fluid Mech.*, 291, 393–407.

Chandrasekera, C. N. (2000). ''Linear refraction-diffraction model for steep bathymetry.'' PhD dissertation, University of Hawaii, Honolulu.

Chandrasekera, C. N., and Cheung, K. F. (1997). ''Extended linear refraction-diffraction model.'' *J. Wtrwy., Port, Coast., and Oc. Engrg.*, ASCE, 123(5), 280–286.

Chen, H. S., and Mei, C. C. (1974). ''Oscillations and wave forces in a man-made harbor in the open sea.'' *Rep. No. 190*, Ralph M. Parsons Lab., MIT, Cambridge, Mass.

Fawcett, J. A. (1992). ''A derivation of the differential equations of coupled-mode propagation.'' *J. Acoustics Soc. Am.*, 92, 290–295.

Kirby, J. T. (1986). ''A general wave equation for waves over rippled beds.'' *J. Fluid Mech.*, 162, 171–186.

Lee, C., Park, W. S., Cho, Y. S., and Suh, K. D. (1998). ''Hyperbolic mild-slope equations extended to account for rapidly varying topography.'' *Coast. Engrg.*, 34(3-4), 243–257.

Lee, C. (1999). ''Discussion of 'Extended linear refraction-diffraction model,' by C. N. Chandrasekera and K. F. Cheung.'' *J. Wtrwy., Port, Coast., and Oc. Engrg.*, ASCE, 125(3), 156–157.

Massel, S. R. (1993). ''Extended refraction-diffraction equation for surface waves.'' *Coast. Engrg.*, 19, 97–126.

Oliveira, F. S. B. F., and Anastasiou, K. (1998). ''An efficient computational model for water wave propagation in coastal regions.'' *Appl. Oc. Res.*, 20(5), 263–272.

Panchang, V. G., Pearce, B. R., Wei, G., and Cushman-Roisin, B. (1991). ''Solution of the mild-slope wave problem by iteration.'' *Appl. Oc. Res.*, 13(4), 187–199.

Porter, D., and Staziker, D. J. (1995). ''Extensions of the mild-slope equation.'' *J. Fluid Mech.*, 300, 367–382.

Suh, K. D., Lee, C., and Park, W. S. (1997). ''Time-dependent equations for wave propagation on rapidly varying topography.'' *Coast. Engrg.*, 32(1), 91–117.

Tsay, T. K., and Liu, P.L.-F. (1983). ''A finite-element model for wave refraction and diffraction.'' *Appl. Oc. Res.*, 5(1), 30–37.

Yue, D. K. P., Chen, H. S., and Mei, C. C. (1976). ''A hybrid element method for calculating three-dimensional water wave scattering.'' *Rep. No. 215*, Ralph M. Parsons Lab., MIT, Cambridge, Mass.

Zienkiewicz, O. C., and Taylor, R. L. (1989). *The finite element method*, 4th Ed., Vol. 1, McGraw-Hill, New York.